Under-ice acoustic navigation using real-time model-aided range estimation

EeShan C. Bhatt,[1,2,a] Oscar Viquez,[2] and Henrik Schmidt[2]

[1]*MIT-WHOI Joint Program in Oceanography/Applied Ocean Science & Engineering, Cambridge and Woods Hole, MA, USA*

[2]*Department of Mechanical Engineering, Massachusetts Institute of Technology, Cambridge, MA*

(Dated: 20 February 2022)

The long baseline (LBL) underwater navigation paradigm relies on the conversion of recorded travel times into pseudoranges to trilaterate position. For real-time operations, this conversion has assumed an isovelocity sound speed. For re-navigation in post-processing, computationally and/or labor intensive acoustic modeling may be employed to reduce uncertainty driven by multipath arrivals. This work demonstrates a real-time ray-based prediction method of the effective sound speed along a path from source to receiver to minimize vehicle position error. This method was implemented for a small scale AUV-LBL system in March 2020, in the Beaufort Sea, in total ice-covered conditions and a double ducted acoustic propagation environment. The vehicle was successfully deployed and recovered. Given the lack of GPS data throughout the vehicle's mission, however, the pseudorange performance is first evaluated on connections between GPS-linked beacons. The real-time ranging error between beacons is roughly 11 meters at distances up to 3 km. But a consistent overestimation in the real-time method provides insights for improved eigenray filtering by the number of surface bounces. An operationally equivalent pipeline is used to re-position the LBL beacons and re-navigate the AUV, using a modeled, historical, and a locally observed sound speed profile. The median re-navigation error is 1.84 $\pm$ 2.19 RMS m. The improved trilateration performance for suggests that this approach effectively extends the single meter accuracy of the deployed GNSS units into the water column.

[a]ebhatt@whoi.edu

I. INTRODUCTION

Autonomous underwater vehicles (AUVs) are increasingly capable platforms to explore and sample the ocean, particularly for remote and/or dangerous regions. However, navigation uncertainty is a major challenge in considering AUVs as standard tools for oceanographic research. While land and air-based robots utilize information from Global Navigation Satellite Systems (GNSS) to achieve stunning location accuracy and precision throughout the duration of their missions, AUVs cannot access GNSS fixes while underwater. Therefore, underwater vehicles have relied on any combination of dead reckoning, hydrodynamic models, inertial navigation systems, doppler velocity logs, and acoustic baseline positioning systems for navigation (Paull *et al.*, 2014). Limiting navigation error and drift requires an AUV to periodically stall on the surface and obtain a GNSS fix to reset its position error. This foolproof method of self-positioning is undesirable for stealth, adverse weather conditions, and mission efficiency, and inaccessible in a GNSS-denied situation like an ice-covered environment.

Of underwater acoustic navigation systems, long baseline (LBL) is the most GPS-like in style and scale, and most appropriate for mitigating drift without overburdening computation or payload size on the vehicle (Van Uffelen, 2021). The state-of-the-art for LBL outsources depth to a pressure sensor and solves the two-dimensional localization problem with an isovelocity, linear scaling between one way travel time (OWTT) and range (Eustice *et al.*, 2006, 2007; Webster *et al.*, 2009, 2012). This assumption is valid for short scale operations but oversimplifies propagation for larger and/or complex acoustic environments.

To achieve single meter, GNSS-like performance in a GNSS-denied environment, we demonstrate an embedded ray-based data processing algorithm to convert recorded OWTTs into pseudorange estimates. This methodology was integrated onto the AUV *Macrura*, deployed and recovered in the Beaufort Sea, in March 2020, during the Ice Exercise 2020 (ICEX20). A physics-driven methodology that received an *in situ* sound speed profile (SSP) was necessary despite the small operational domain because of the relatively high-risk mission environment—total under-ice conditions and a variable double ducted acoustic environment.

For consistency, we delineate specific definitions for timing, positioning, and navigation from Howe *et al.* (2019).

1. Timing is the ability to acquire and maintain accurate and precise time anywhere in the domain of interest within user-defined timeliness parameters

2. Positioning is the ability to accurately and precisely determine one's location referenced to a standard geodetic system

3. Navigation is the ability to determine current and desired position (relative or absolute) and apply corrections to course, orientation, and speed to attain a desired position anywhere in the domain of concern

Thus, navigation is inherently in real-time and depends on positioning; positioning depends on timing. We also suggest re-navigation and re-positioning as post-processed corollaries, which may include knowledge or processing capabilities not available *in situ*.

While RAFOS floats championed one way ranging for re-positioning (Duda *et al.*, 2006; Rossby *et al.*, 1986), the ability to do so for navigation was facilitated by the advent of the WHOI Micro-Modem (Singh *et al.*, 2006) and synchronized clocks (Rypkema *et al.*, 2017). AUV navigation efforts have achieved root mean square (RMS) localization error on the order of tens of meters relative to GNSS surface position over less than ten kilometers in shallow (Claus *et al.*, 2018; Eustice *et al.*, 2007; Kepper *et al.*, 2017) and deep water (Jakuba *et al.*, 2008; Kunz *et al.*, 2008; Webster *et al.*, 2009). However, these efforts all used a nominal sound speed for travel time conversion and the vehicles were limited to shallower isovelocity regimes.

Localization algorithms that do consider environmental or acoustic uncertainty tend to focus on longer and larger experiments, where spatio-temporal variability cannot be ignored. These methods have also been reserved for post-processing as they can be labor intensive, computationally heavy, and/or require additional information like contemporaneous data. For example, gliders navigating with kinematic flight models and equipped with acoustic modems were later unambiguously associated with predicted ray arrivals, resulting in roughly a kilometer error and hundred meters uncertainty over basin scale propagation (Van Uffelen *et al.*, 2013). A follow up study investigated how a single temporally and spatially averaged SSP could mitigate position error for a four month glider mission (Uffelen *et al.*, 2016). Wu *et al.* (2019) cross correlate three days of real acoustic records with synthetic ones generated through ocean model snapshots from HYCOM (Chassignet *et al.*, 2007). While potentially applicable for various ocean states, this is reliant on model realism and impractical for real-time operations. Mikhalevsky *et al.* (2020) introduces a "cold start" algorithm that does not require prior knowledge of track, position, or sound speed information. The algorithm inputs a four-dimensional ocean model, constrained by tomography data, into a range dependent ray code to isolate the last path detected in a full multipath pattern. Then, a representative group speed is solved for alongside position in a least squares fashion. This approach is able to re-position a floating hydrophone array with an error of 58 m and a standard deviation of 32 m based on six sources 129–450 km away but remains to seen for real-time navigation.

The ICEX20 AUV deployment necessitated an environmentally- and physically-driven relationship between recorded travel times and estimated pseudoranges due to the multipath uncertainty brought upon by an increasingly observed double ducted environment in the Beaufort Sea, which some refer to as the "Beaufort Lens" (Chen *et al.*, 2019; Chen and Schmidt, 2020; Litvak, 2015).

Given that a lens introduces significant ray refraction, the Beaufort Lens is a shorthand for the spatio-temporal variability of the local temperature and sound speed maxima generally around 50 to 60 m in depth. A neutrally buoyant layer of warm Pacific Summer Water creates a unique double ducted environment —the upper duct degrades signal coherence due to intensified ice interaction and the lower duct effectively traps sound for long range propagation (Poulsen and Schmidt, 2017). Modeling output (Duda *et al.*, 2021, 2019) and experimental observations (Ballard *et al.*, 2020; Bhatt, 2021) suggest that, in the Beaufort Sea, the duct is persistent and widespread but not necessarily continuous; it and its acoustic effects can be non-existent, minimal, or drastic. Transmissions in the upper duct, between the surface ice and the lens, experience minimal attenuation but degrade in signal coherence with repeated reflections under the ice. In lower duct, between the lens and its conjugate depth in the Atlantic water, roughly 200 m, sound above 350 Hz is trapped near losslessly for long range propagation (Poulsen and Schmidt, 2017).

Thorough reviews of uncrewed vehicle operations in polar environments can be found in (Norgren *et al.*, 2014) and (Barker *et al.*, 2020); there is no comparable work in the Arctic for a short range AUV deployment in the Beaufort Lens. Seminal (Bellingham *et al.*, 1995; Brooke, 1981; Hayes and Morison, 2002; Jackson, 1983; Light and Morison, 1989) and more recent AUV deployments (Fossum *et al.*, 2021; Jakuba *et al.*, 2008; Kukulya *et al.*, 2010; Kunz *et al.*, 2008; Plueddemann *et al.*, 2012; Timmermans and Winsor, 2013) witnessed the classical upward refracting sound speed profile that is amenable to an isovelocity assumption.

Of note, despite different platforms and scales, are recent glider deployments in the Canada Basin. In 2014, in partially ice-covered conditions, a long range LBL system with WHOI Micro-Modems at 100 m exploited the lower duct for long range communication with two gliders (Freitag *et al.*, 2016; Webster *et al.*, 2015). The sound speed value measured at the time of reception was used to estimate pseudorange in post-processing. The beacon-to-beacon performance was excellent, achieving contact at ranges greater than 200 km with a position uncertainty of 40 m. The beacon-to-glider performance, however, deteriorated due to missed contacts outside the duct, and was not described quantitatively. In 2017, gliders were deployed in a region with no ice coverage (Graupe *et al.*, 2019). Ranges were linearly scaled by a statistical description of sound speed observations taken during the experiment, 1450 $\pm$ 6.5 m/s. This resulted in an error of 550 m, which was reduced by a factor between 4 and 5, depending on the dive, using a post-processing acoustic arrival matching method. Both cases exploit the lower duct for high fidelity communication at long ranges. Unintuitively, the smaller nature of our deployment during ICEX20 is not a simplifying factor. For source depths typical to vehicle operations, 30 to 200 m, a shadow zone spans from 2 to 6 kilometers in range (Schmidt and Schneider, 2016).

Compared to the previous small scale navigation efforts, the approach in this paper integrates real-time model-aided data processing to estimate a representative sound speed along a path from source to receiver, leveraging climatology, *in situ* data, and fast acoustic modeling. The paper is organized as follows. Section II details the experimental approach and conditions during ICEX20. Given that there is no GNSS ground truth for the vehicle position while underway, we first evaluate the real-time ranging performance of GPS-linked beacon-to-beacon communication events in section III. Section IV uses insights from field data to introduce a new ray filtering algorithm to improve range estimation. Section V emulates the real-time processing pipeline to re-position beacon-to-beacon events and re-navigate AUV *Macrura*.

II. OVERVIEW OF THE ICEX20 EXPERIMENT

The results from this paper derive from data taken while deploying the AUV *Macrura*, a custom Bluefin-21, during the Ice Exercise 2020 (ICEX20), in the Beaufort Sea, from March 8th to 11th. The AUV deployment was supported by the Integrated Communication and Navigation Network (ICNN) (Randeni *et al.*, 2020, 2021; Schneider *et al.*, 2020), a specialized implementation of the LBL solution. The ICNN was initially developed via numerous virtual experiments to ensure robust algorithms and interfaces between different hardware components. The simulation capabilities are largely physics-driven with a modular system of systems approach—an environmental simulator with sub-components for the ocean, including Arctic ice drift and ocean acoustic propagation; a vehicle simulator with sub-components for vehicle dynamics and navigation; a topside hardware simulator and acoustic communications simulator, both with a software-only configuration and a hardware-in-the-loop version (Schneider and Schmidt, 2018). The virtual environment similarly emulates the interfaces between the real components to test the entire software pipeline.

A. The Integrated Communication and Navigation Network

The ICNN is comprised of four ice buoys in a loose rectangle, roughly 2 km away from a central ice camp with a topside computer, as shown in Fig. 1. The AUV and each ice buoy are outfitted with a WHOI Micro-Modem (Singh *et al.*, 2006), with a four-element receiver array, a single transmitter, and one-tenth of a millisecond resolution. Acoustic messages were sent with a 10 kHz carrier frequency, 5 kHz bandwidth, and phase-shift

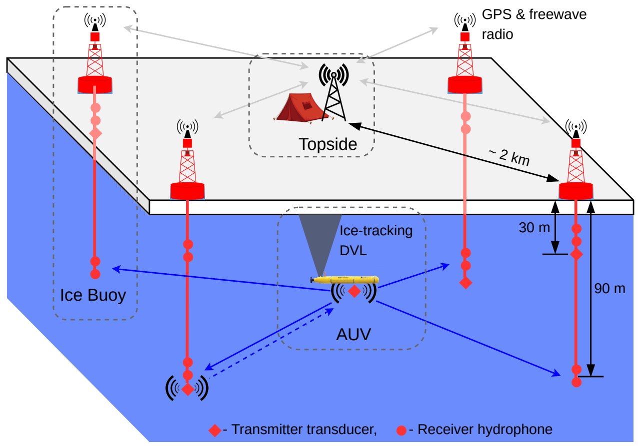

FIG. 1. A schematic overview of the Integrated Communication and Navigation Network (ICNN), which provides joint data-transfer and tracking between AUV and a human decision maker at Topside.

keying (PSK)modulation on a time-division multiple access schedule with a thirty-second cycle, giving room for two-way communication throughout the mission volume. The receive and transmit elements were split between shallow and deeper depths—30 and 90 m—to provide better coverage across the shadow zone. While each buoy only has one transmit depth, all buoys have both receive depths but the active receive layer is consistent across all buoys. The design of the ICNN enables a self-adapting network to transmit and receive at the optimal depth to maintain contact with the AUV (Schneider *et al.*, 2020). The buoys do not encompass the full horizontal range of the vehicle but are positioned to minimize overlap in trilateration for spherical positioning (Deffenbaugh *et al.*, 1996a).

To balance competing uses of the acoustic channel, the network uses a single synchronized digital communication packet to provide both tracking and data to the operator.

1. The AUV, running an ice-tracking DVL and an onboard hydrodynamic model, broadcasts its perceived location on a scheduled, time-synchronized message via WHOI Micro-Modem

2. Four ice buoys, each outfitted with a WHOI Micro-Modem, receive messages from the AUV and send that information over freewave radio to a Topside computer

3. The topside computer converts travel times into pseudorange estimates using a stochastic embedded prediction of the horizontal group velocity via BELLHOP ray tracing code (Porter, 2011) using a sound speed profile provided by an updatable Virtual Ocean (Bhatt *et al.*, 2022; Schneider and Schmidt, 2018)

4. The topside computer calculates a new position by trilaterating the range estimates

5. The position differential, not the absolute position, is broadcast to the vehicle to update its navigation solution and be robust to latency and intermittency

In the face of GNSS-denied navigation, this approach was anecdotally successful, as shown in Fig. 2. The AUV *Macrura* was deployed through a hydrohole from an ice camp but recovered through an emergency hydrohole. A random disk error stalled *Macrura* underneath the ice but did not prevent it from transmitting its location. Due to an incoming storm, a team placed a physical marker on the ice at the location. Three days later, *Macrura* was found within a meter of the marker. We view the emergency recovery as qualitative proof of the robustness of this navigation approach. Nonetheless, this paper specifically addresses the third and fourth steps—the conversion of travel times into pseudoranges and its effect on trilateration. By focusing on pseudorange estimates between GPS-tracked beacons, and re-running the trilateration pipeline, the results are decoupled from all other mechanisms in the ICNN.

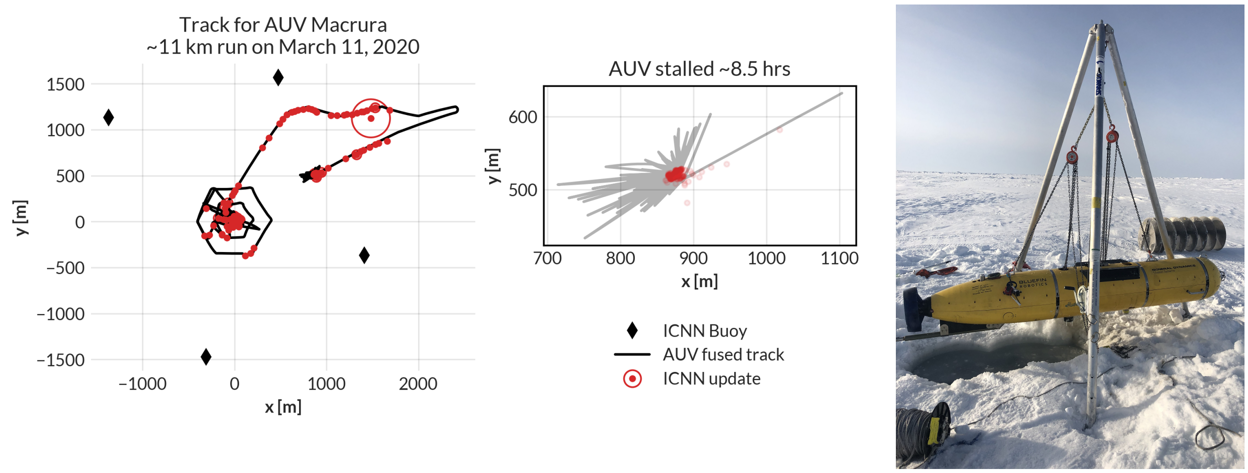

FIG. 2. The under-ice mission track for AUV *Macrura*, including the position updates as it stalled underneath the ice overnight. A marker was placed on the ice at the vehicle's estimated self-location. It was recovered after a three day storm within a meter of the marker.

B. ICEX20 sound speed conditions

An important component to our navigation solution is an accurate estimation of a representative SSP for the ocean volume. Previous field experience, during the Ice Exercise 2016 (ICEX16), demonstrated the negative effects of the Beaufort Lens on tracking and communication (Schmidt and Schneider, 2016). Fig. 3 shows historical, modeled, and *in situ* sound speed data for both ICEX16 and ICEX20. These three input streams were selected to mirror the information available on a submarine (personal conversation with LT B. Howard and LT CDR D. Goodwin). In the field, the SSP information was shared with the vehicle via basis representation compression on a lightweight digital acoustic message (Bhatt *et al.*, 2022). All modeled data comes from HYCOM (Chassignet *et al.*, 2007), which does not seem to capture the forcing mechanisms that cause the Beaufort Lens. For ICEX16, the data-driven profile was sourced from nearby Ice Tethered Profilers (ITP) after the field experiment (Krishfield *et al.*, 2008; Toole *et al.*, 2011) and exhibits a fairly low lens; the historical profile is from the World Ocean Atlas. For ICEX20, the chosen weights (data-driven) profile derives from an estimate of initial CTD casts taken on site, showing an intense warm water intrusion; the baseline (historical) profile, showing moderate ducted conditions, comes from the average of March 2013 ITP data. This month best matched sea ice and sound speed conditions at the beginning of ICEX20 (Bhatt *et al.*, 2022). It is important to note that all profiles that do show the Beaufort Lens do so with different local sound speed maxima at different depths, reflective of the wide range of lens properties observed for all ITP data in the region. The variability of the lens height and prominence is the main reason an updatable SSP was integrated into the ICNN solution.

During ICEX20, the HYCOM profile was available but never deployed. For post-processing comparison, we introduce both the HYCOM profile and an isovelocity case, 1441.8 ± 3.7 m/s, as the mean and standard deviation of the observed sound speed profile over the first 200 m.

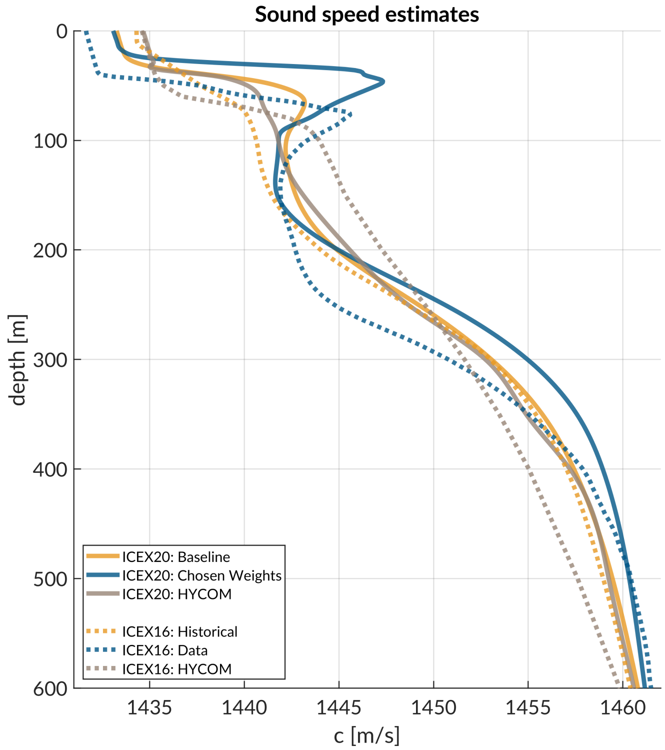

FIG. 3. Sound speed conditions for historical (baseline), data (chosen weights), and HYCOM model for both ICEX16 and ICEX20.

III. REAL-TIME PSEUDORANGE ANALYSIS

Because the vehicle's navigation solution during a mission can only be evaluated on the basis of the error estimates sent, a sister experiment for validating the real-time ranging approach was implemented. Ice buoy modems were run as "virtual vehicles" at a fixed depth, receiving position updates from the other beacons as well as a camp site modem lowered to 20 m. Figure 4 shows successful events sorted by source depth. In this analysis, we assume there is insignificant displacement between the GNSS puck surface expression and subsurface modem; this is supported by unusually low observed ice drift rates, just 0.7 cm/s on average throughout the mission.

A. Minimal bounce criteria (MBC)

The fundamental challenge to implement GNSS-like navigation, especially in an acoustically complex propagation environment, is characterizing a single sound speed to compensate for the effects of ray refraction and reflection. The use of the acoustic modem network for tracking relies on the accurate estimates of travel times between the submerged platform and LBL beacons, supported by clock synchronization and a pre-determined scheduling of acoustic events. For the Beaufort Lens in particular, the strong multipath effects make it virtually impossible to deterministically predict the modem's detected arrival time.

Instead, for each individual modem i, an embedded stochastic tracking framework is used to provide a running estimate of the effective sound speed $c_{i,j}$ for the conversion from travel time to range from modem j, with the ultimate goal of matching the implied horizontal

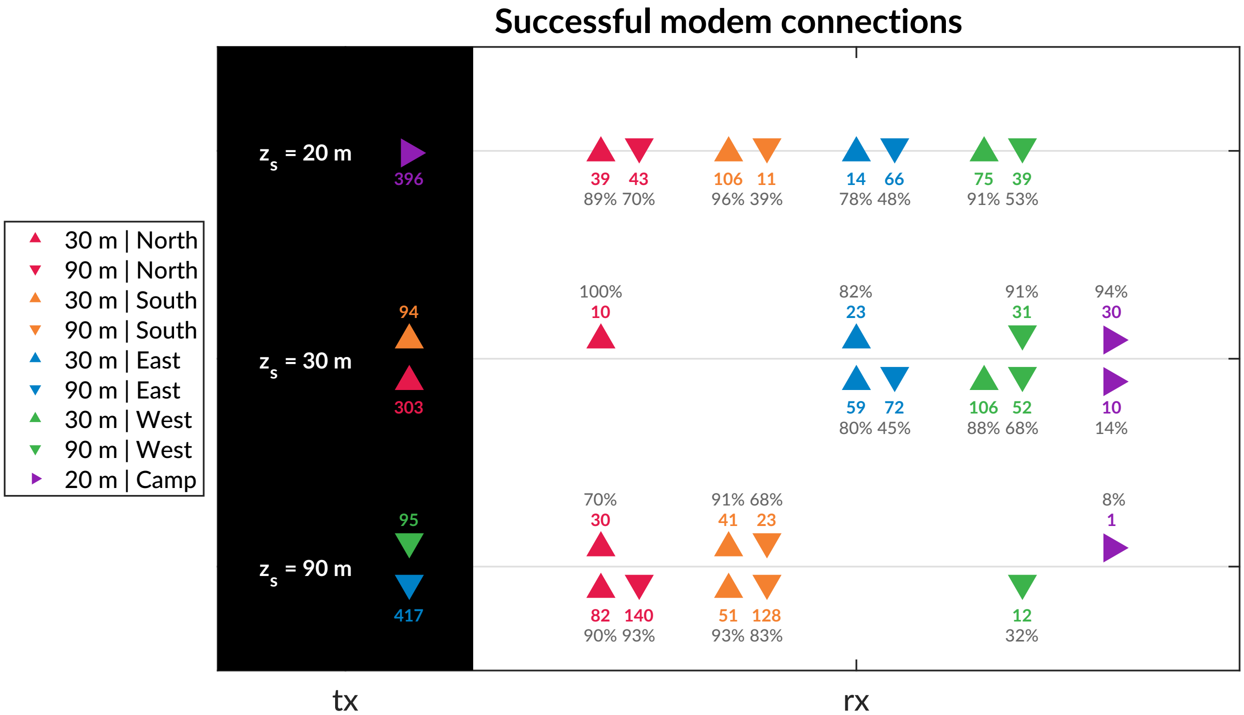

FIG. 4. An overview of the modem experiment by source and receiver depth and position. The black column on the left, *tx*, shows the source depth, z_s, with the total number of transmissions. The column on the right, *rx*, shows the receivers with the number of successful decodings and the percent success rate, defined as the ratio of decoded to detected. The orientation of the triangles—sideways, upwards, and downwards—corresponds to depths of 20, 30, and 90 m.

effective sound speed, i.e., the GPS-recorded distance between two nodes divided by the modem-recorded one way travel time between them.

In the ICEX20 configuration, the acoustic tracking is running on the topside computer, which controls the ICNN. Here we assume that the effective sound speeds $c_{i,j}$ are smoothly varying over the course of a vehicle mission, i.e., with respect to range, mission time, and the thirty-second frequency.

When the topside tracking framework receives a message, with a time delay, Δt, it will request a new estimate for $c_{i,j}$ along with its standard deviation. The effective sound speed is predicted using the vehicle's reported depth and the extrapolated navigation solution for range, $\hat{r}$, as inputs to the ray tracing program, which returns an impulse response estimate in the form of ray travel times dt_j and amplitudes a_j.

The initial call to BELLHOP is over a local grid centered at the range and depth posited by the onboard tracking solution. The grid, compared to a point solver, adds redundancy in resolving the actual multipath structure for a reliable acoustic path without overtaxing onboard computational time and memory. It is initialized as 11 $\times$ 11 points spanning 10 m horizontally and 20 m vertically. The horizontal dimension reflects the accumulated vehicle position error given a thirty-second communication cycle; the vertical dimension reflects how, computationally, eigenrays of the same timefront seem to stack vertically in the water column. For each grid point, BELLHOP produces a number of arrivals resulting from multiple propagation paths. Using only the N_0 rays with neither surface nor bottom bounces, it will then estimate the current effective sound speed c from a power weighted average of the ray travel times,

$$c = \frac{\hat{r}\sum_{n=1}^{N_0} a_n^2}{\sum_{n=1}^{N_0} dt_n a_n^2} \ , \tag{1}$$

and the associated weighted standard deviation,

$$\sigma_c \simeq \sqrt{\frac{\sum_{n=1}^{N_0}(dt_n - \hat{r}/u)^2 a_n^2}{\sum_{n=1}^{N_0} a_n^2}}\,\frac{u^2}{\hat{r}} \tag{2}$$

If no direct paths exist, i.e. $N_0 = 0$, then the effective speed is computed using the same algorithm for the ray arrivals with one bounce, and so on.

Finally, the pseudorange is calculated simply as

$$r_{i,j} = c_{i,j} \Delta t_{i,j} \tag{3}$$

Thus the MBC method assumes the signal detected by the modem will be dominated by a set of paths with the least number of boundary interactions. Importantly, this stochastic, ensemble method for group velocity calculation can run in real-time, appearing to be orders of magnitude faster than other post-processing methods which seek to determine the specific ray itself that best matches a prominent indicator from the arrival structure. The BELLHOP simulation that runs this calculation uses 3600 rays with launch angle fan of -60 to 60 degrees, a representative depth dependent sound speed profile, and a range dependent bathymetry.

B. Pseudorange error metrics

The sister modem experiment generated 811 beacon to beacon communication events with their own real-time MBC group velocity predictions. Given the complexity of the ICNN system, this experiment did not collect an exhaustive set of data across all buoy, source depth, receive depth, and sound speed combinations. The algorithm generally overestimates pseudoranges because it resolves the effective sound speed for the most direct path.

Fig. 5 shows the range error boundary for both SSP inputs used in ICEX20. A promising sign that the MBC method adapts sound speed somewhat intelligently is the lack of error growth as travel time increases. The baseline SSP (n=243 events) has an absolute pseudor-

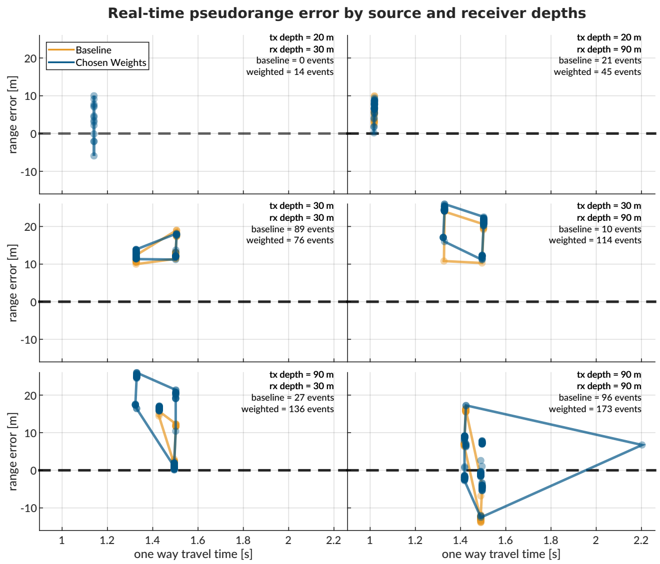

FIG. 5. The real-time range error by source (rows: 20, 30, and 90 m) and receiver (columns: 30 and 90 m) pairings for both sound speed estimates used during ICEX20. The amount of communication events is notated in the top right of each panel. The dashed line indicates no range error, and the boundary drawn indicates scope of the range error as a function of one way travel time.

ange error of 11.38 ± 4.23 m; the weighted SSP (n=568), 11.36 ± 8.12 m. The discrepancy between these two is largely due to outlier events only contained in the weighted SSP set. Where there is overlap between sound speed conditions used for the real-time MBC, the pseudorange error difference is no more than a few meters. The overarching results show that sound speed estimates derived from eigenrays for a local grid, as opposed to a singular point, are accurate enough to support vehicle navigation. While the NBC looks for just the least complex multipath, the high density of launch angles almost always guarantees a direct path. Nonetheless, the consistent overestimation of pseudorange invites further analysis into acoustic arrival matching.

C. Eigenray identification for beacon-to-beacon events

Accounting for ice movement between beacons creates nominal ranges with small variability. Figs. 6, 7, and 8 show eigenrays for three sound speed environments for source depths of 20, 30, and 90 m, respectively. Eigenrays were initially found using the built-in BELLHOP protocol with a launch angle fan of 2400 rays between -60 and 60 degrees. Separately, recorded travel times between beacons were clustered with 1 millisecond boundaries such that some source-receiver pairs had multiple, distinct travel times to approximate. The BELLHOP eigenray returns were then filtered such that one was selected per travel time cluster, in the hopes that the eigenray will converge to the receiver locations for the most realistic sound speed input. It should be noted that bottom bounces were recovered but filtered out. The three source depths create distinct ray geometries with respect to the three sound speed inputs.

1. Source depth of 20 m

For a source at 20 m in depth, shown in Fig. 6, reliable eigenrays are found for all sound speed inputs. Rays refract upwards and neatly intersect with the shallow and deep receiver locations between 1.5 and 1.8 km in range. However, the ray paths for the shallow receivers change both in the number of surface interactions and where the surface interactions occur with respect to range across the SSPs. As the Beaufort Lens strengthens, the chosen paths to the second farthest shallow buoy (North, in red) interact with the surface more and become distinct. The weighted SSP shows the most interesting effects for the deeper receivers. The

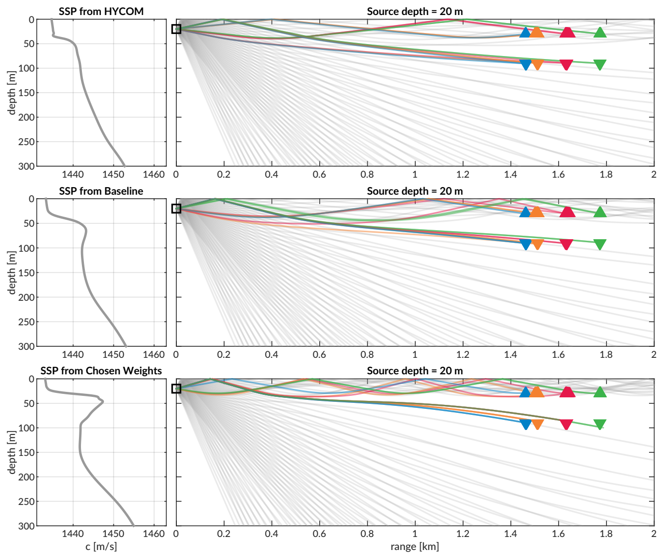

FIG. 6. Eigenrays for beacon-to-beacon events for each sound speed with a nominal source depth of 20 m over a total ray fan in gray. The beacons are highlighted in color/marker coding in Fig. 4.

ray paths all interact with the surface and the eigenrays for the Northern (red) and Western (green) buoys are in fact the same ray.

2. *Source depth of 30 m*

The ray geometries from the 30 m source, shown in Fig. 6, show a similar degradation of eigenray identification with increased ducting. Receptions span 1.5 to 3.2 km. Once again, eigenrays for HYCOM and the baseline SSP are visually appropriate. Rays for the weighted SSP show how the surface channel intensifies ice interactions and how the shadow zone denies reliable acoustic paths. Pointedly, the increasing number of surface reflections to the farthest shallow buoy (North, in red) crystallize the MBC's tendency for overestimation. For the HYCOM, baseline, and weighted SSP inputs, the most appropriate eigenrays show 2, 3, and 4 surface interactions.

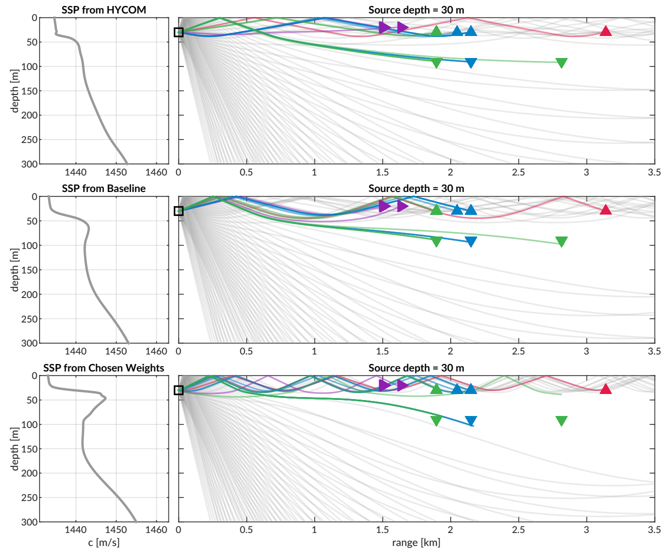

FIG. 7. Eigenrays for beacon-to-beacon events for each sound speed with a nominal source depth of 30 m over a total ray fan in gray. The beacons are highlighted in color/marker coding in Fig. 4.

322 ### 3. *Source depth of 90 m*

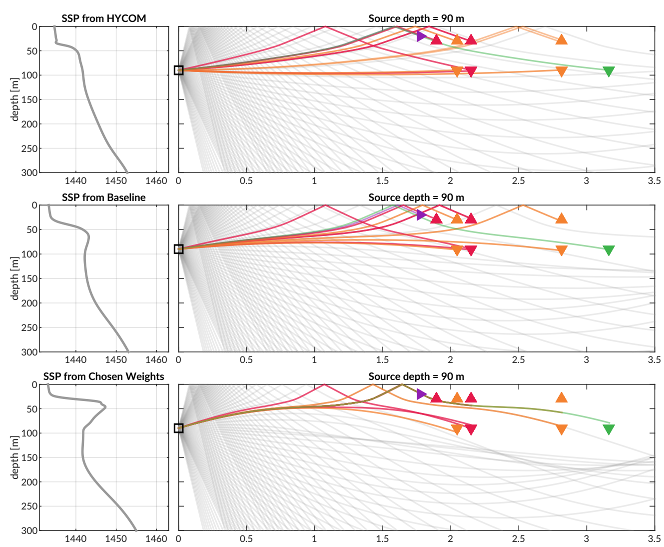

FIG. 8. Eigenrays for beacon-to-beacon events for each sound speed with a nominal source depth of 90 m over a total ray fan in gray. The beacons are highlighted in color/marker coding in Fig. 4.

Lastly, Fig. 8 shows ray geometries from the 90 m source, elucidating a different extent of the shadow zone. While the receiver locations are similar to that of the 30 m source depth, the deeper source depth effectively negates the upper duct and places the upper (and some of the lower) receivers in unreliable acoustic paths. The HYCOM eigenrays still show the most reliable acoustic paths that deteriorate with increasing ducted conditions. The lack of direct paths from the observed SSP further points out the shortcomings of the MBC approach.

The goal of the MBC algorithm was to provide a reliable, physically intuitive interpretation of the acoustic propagation without taking on the additional burden of regularly identifying specific paths that may connect any given source-receiver pair in the network. Its performance was adequate for vehicle navigation and would have likely sufficed if it were not for the prominence of the duct observed relative that of other model and data products.

IV. POST-PROCESSED PSEUDORANGE ANALYSIS

From all events recorded during the modem test experiment, there are 1242 successfully decoded beacon-to-beacon events. Only these events are used to evaluate ranging accuracy, as the ICNN was not configured to use receptions with failure flags. Thus, a post-processing analysis that emulates the real-time navigation engine was run to overcome the unequal distribution of communication events with respect to depth, range, and sound speed status.

It is important to note that the value for the extrapolated range, $\hat{r}$, is only tracked when the modem runs the vehicle behavior; thus we replace $\hat{r}$ with the GPS-tracked range for all modem events. Because $\hat{r}$ converges to the correct solution, a comparison of $\hat{r}$ with the GPS-tracked range shows a normal, zero-centered distribution within the bounds of GPS drift. The present analysis therefore seeds realistic but "omniscient" knowledge of the extrapolated range and leverages the post-processing pipeline to more thoroughly evaluate the acoustic range estimate for all modem events, with three relevant sound speed sources, and both group velocity criterion. Accordingly, the results in this section evaluate the utility of the algorithms and sound speed sources, divorced from their role in the ICNN while maintaining real-time relevance.

A. Nearest bounce criteria (NBC)

As shown in the eigenray traces of Fig. 7, the extent of ray bending and repeated reflections is extremely dependent on the sound speed profile. An isovelocity approach would completely miss this nuance; our field-tested approach that only resolved the simplest path is unlikely to resolve the one that triggers modem detection. Based on this insight, a new algorithm, the nearest bounce criteria (NBC), is a slight modification from the MBC and includes multipath as a new dimension of information to exploit. This metric, while run in post-processing, adds a negligible amount of computation for real-time efficacy.

Given a running estimate for the horizontal group velocity $u_{i,j}$ between nodes i and j, the navigation system has an extrapolated value for range, $\hat{r}$, and a recorded travel time, $\Delta t_{i,j}$. Instead of using only the N_0 rays with neither surface nor bottom bounces to estimate group velocity and subsequently moving to incremental number of bounces only when no valid direct path solutions exist, we solve for the power weighted average of the ray travel time for the N_k rays with k bounces,

$$t_k = \frac{\sum_{n=1}^{N_k} dt_n a_n^2}{\sum_{n=1}^{N_k} a_n^2} , \tag{4}$$

find the nearest matching power weighted average to recorded travel time,

$$t_{i,j,k} = \min_{k=0,1,2,\ldots} |t_k - \Delta t_{i,j}| \tag{5}$$

predict a group velocity,

$$u_{i,j} = \frac{\hat{r}}{t_{i,j,k}} \tag{6}$$

and estimate the range as was done previously.

$$r_{i,j} = u_{i,j} \Delta t_{i,j} \tag{7}$$

This method selects a different group velocity based on the multipath arrival structure, as the detected arrival is not always the first arrival or the direct path and could even be masked by noise or blocked temporarily (Deffenbaugh *et al.*, 1996b). We manually cap the number of bounces to 4 because of the smaller operational scale and the attenuation accrued with many surface interactions. Bottom bounces are not encoded separately because of ray's tendency to refract upward, not due to information limitations.

B. Effective sound speed predictions

The minimal and nearest bounce algorithms are applied with the three sound speed inputs shown in Fig. 7. The resulting predicted group velocities for all source depths are shown in Fig 9.

The goal of the group velocity estimation is to converge towards the implied sound speed, i.e. the GNSS-derived range divided by the recorded travel time. For a 30 m receiver depth, the NBC shows more overlap with data-derived values as it classifies multipath more correctly. For a 90 m receiver depth, the overlap is less accurate due to computational constraints of a limited fan of rays entering the shadow zone rendering a less reliable simulated times of arrival packet.

As the environmental and ray filtering method become better representations of the real ocean, the lower the expected mismatch is between the implied and estimated effective sound speeds. Analysis shows that the higher multipath classification produces more accurate sound speed predictions, likely driven by a tighter and/or sparser bundle of rays. However, that data are too small to draw significant conclusions. Discontinuities in multipath classification verify our hypothesis for its importance to a smoothly varying group velocity, as shown in the cluster for a receiver depth of 30 m, where HYCOM jumps from

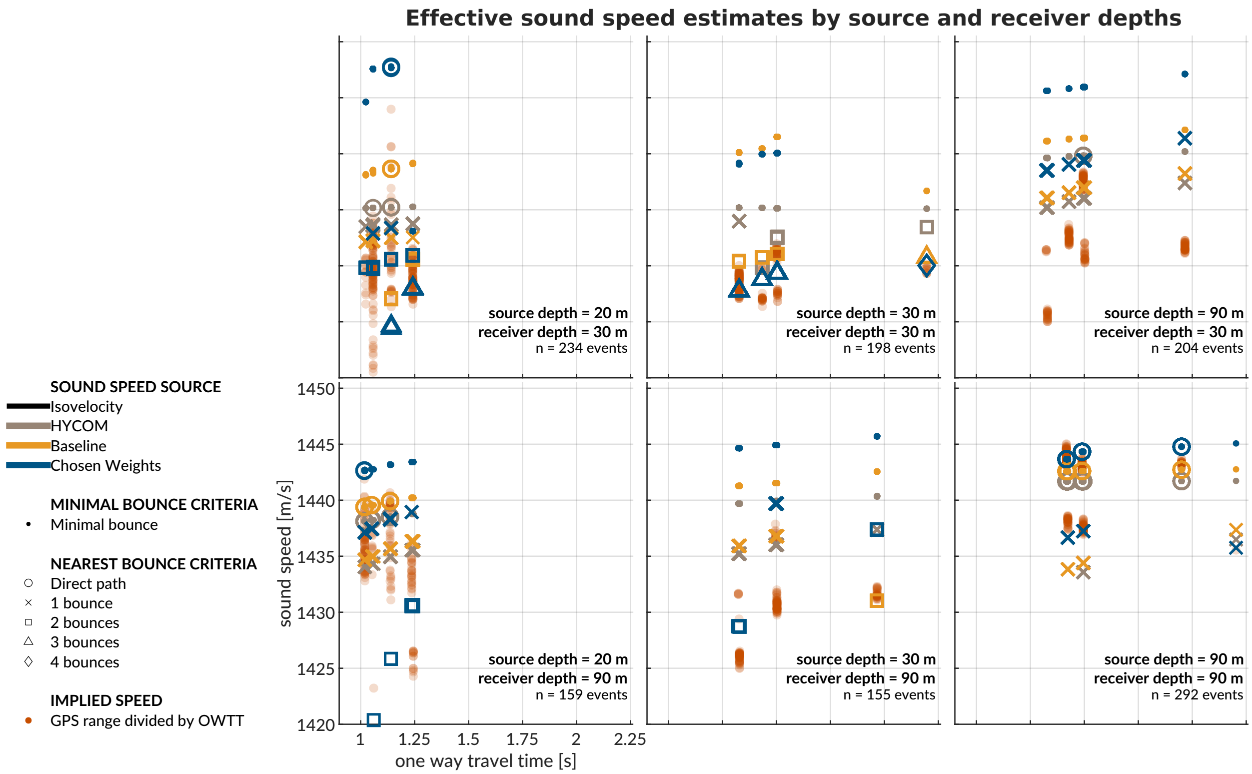

FIG. 9. A comparison of group velocity predictions for all beacon to beacon events in post-processing with a source depth of 30 m, with group velocity on the y-axis and recorded travel time on the x-axis. The left panel is for a receiver depth of 30 m; the right panel for 90 m. The sound speed source is indicated by color. The minimal and nearest bounce criterion are distinguished by different marker shapes, compared to the separately colored red dots showing the naive, data-driven group velocity calculation.

one to two bounces amidst the baseline SSP and weighted SSP smoothly increasing while consistently seeing two and three bounces, respectively.

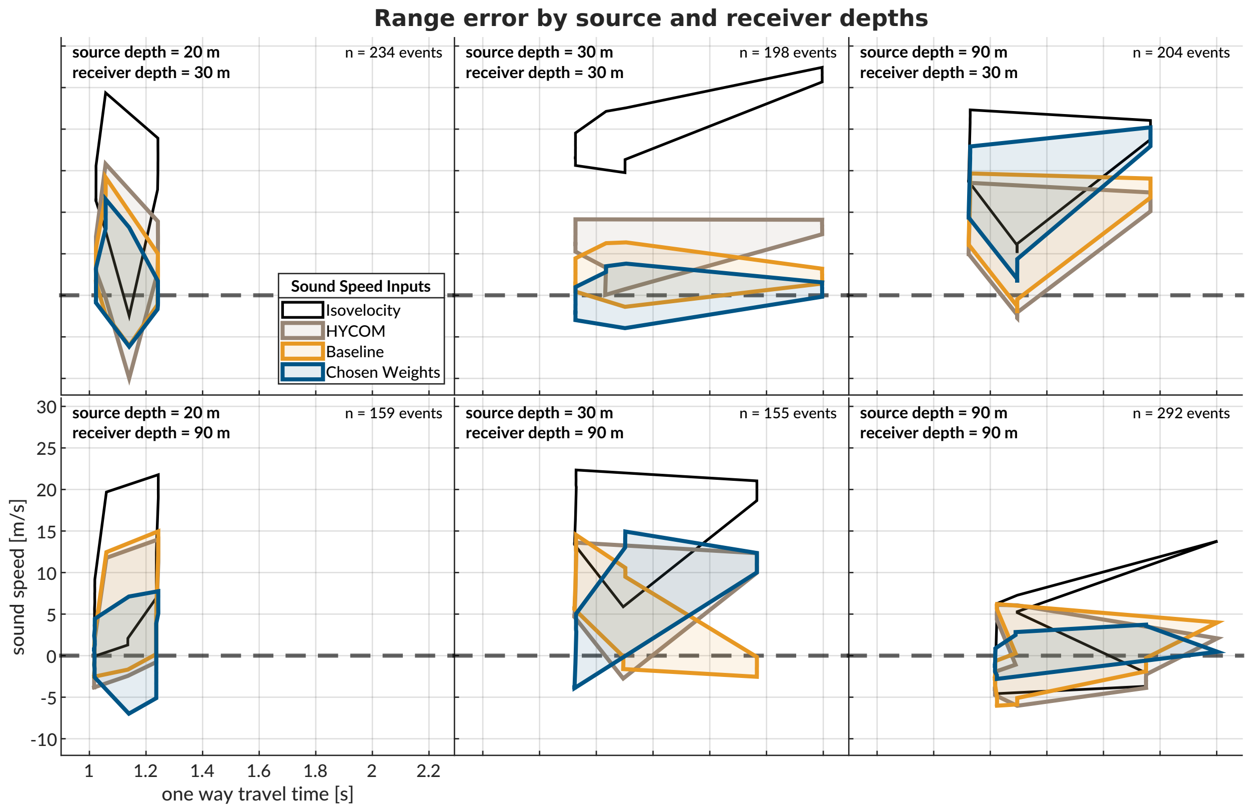

FIG. 10. The post-processed range error for source depths of 20, 30, and 90 m, and receiver depths of 30 and 90 m. The dashed gray line shows no error. The shaded region connects the range performance across all events.

C. Pseudorange error metrics

Fig. 10 shows the directional range error footprints for all three sound speed inputs with respect to OWTT, separated by source and receiver depth configurations. The weighted SSP range error generally has the smallest and most zero-centered footprint. The one case it does not is for the source-receiver pairings between 30 and 90 m in depth. The increased error for these reciprocal transmission paths is most likely driven by the computational artifacts encountered when propagating through the steep sound speed gradients of the lens and through the shadow zone. All other source depth pairings are significantly improved using the chosen weights compared to HYCOM or the baseline.

When using a linear scaling to convert travel time into range, any offset between the assumed sound speed and the horizontal group velocity produces unconstrained error with increasing receiver distance. Most importantly, we see the consequences of the adaptive group velocity in that range error does not strictly increase with OWTT.

The improvement from MBC to NBC is most evident for the realistic sound speed; while the HYCOM SSP improves from a median absolute range error of 6.41 to 4.61 m, the baseline SSP improves from 10.30 to 2.27 m, and the weighted SSP improves from 13.28 to 2.12 m. Table I shows further statistics on the absolute range error by SSP and group velocity algorithm. The order of magnitude improvement in the ducted SSPs demonstrate the effectiveness of the algorithm exploiting the multipath conditions.

As shown in table I, there is a striking maximum range error of 1491 m for the weighted SSP in the minimal bounce criteria. There are 10 events from South transmitting at 30 m depth to North receiving at 30 m depth. The OWTT spread is from 2.1958 to 2.1963 s; the naive group velocity is 1429.3 to 1430.1 m/s; and the GPS-tracked range is from 3138.54 m to 3140.87 m. This example ends up being an excellent case study for how sound speed and multipath fidelity work in concert to minimize range error. The large error in this instance is driven by the MBC unexpectedly defaulting to a bottom bounce with a much greater OWTT. The NBC classifies the multipath as 4 bounces, reducing the range error from greater than a kilometer to less than a meter. While there is no actual way of knowing if this is the correct multipath structure, the range error is remarkably small, at 0.025%. This

	Baseline		**Chosen Weights**		**HYCOM**	
	MBC	NBC	MBC	NBC	MBC	NBC
minimum [m]	0.01	0.00	0.00	0.00	0.11	0.01
25th % [m]	4.96	0.99	6.26	0.95	3.30	2.25
median [m]	10.30	2.27	13.28	2.12	6.41	4.61
75th % [m]	15.81	5.51	19.75	4.11	10.92	7.46
maximum [m]	22.52	14.96	1491	20.21	19.55	15.81

TABLE I. A comparison of range estimation metrics for each sound speed source and group velocity estimation algorithm for all 1283 beacon to beacon events via post-processing. The 0th (minimum), 25th, 50th (median), 75th, and 100th (maximum) percentiles are shown to the range resolution afforded by the WHOI Micro-Modem. There are a few outliers that drive the mean to be higher than the median.

pattern of not choosing the minimal observed bounce structure is consistent across all SSPs; the baseline goes from 1 to 3 bounces and HYCOM goes from 0 to 2 bounces. Notably, the baseline and HYCOM range errors are never egregiously large, but are nonetheless improved with the NBC algorithm. Thus, for acoustically complex environments, the NBC has a disproportionately positive impact as the estimated SSP approaches the desired SSP.

V. TRILATERATION FOR ICEX20 FIELD DATA

To overcome potentially intermittent acoustic communication, the operational paradigm of the ICNN computes corrections relative to the trilaterated position estimates transmitted by the vehicle, rather than transmitting the updated positions themselves. The reliability of the correction is directly linked to how accurately the travel time measurements are converted to pseudoranges. This section aims to resolve that tension by reevaluating the trilateration results with respect to the MBC and NBC algorithms. The MBC/NBC sound speed estimates were tracked independently for each transmitter-receiver pair; although the sound speed was expected to be locally smooth near a given receiver, no such assumption was enforced between distinct acoustic links.

A. Re-positioning beacon to beacon events

When the beacons ran as virtual vehicles, the ICNN did not have access to that buoy's GPS data stream except for what was sent via digital acoustic message. The static nature of the experiment means that the initial estimate transmitted to the ICNN was in fact a ground truth position. Therefore, a distribution of corrections from the ICNN, as shown in Fig. 11, reflects positioning accuracy. The NBC clearly outperforms the MBC, with almost 80% of the corrections below 6 meters and the median within the deployed GNSS puck precision of 3 meters. By contrast, the MBC shows roughly 20% within the GNSS puck precision, and separate peaks from 9–12 meters and 21–27 meters. This trimodal nature reflects the distribution of reflections on the ice surface.

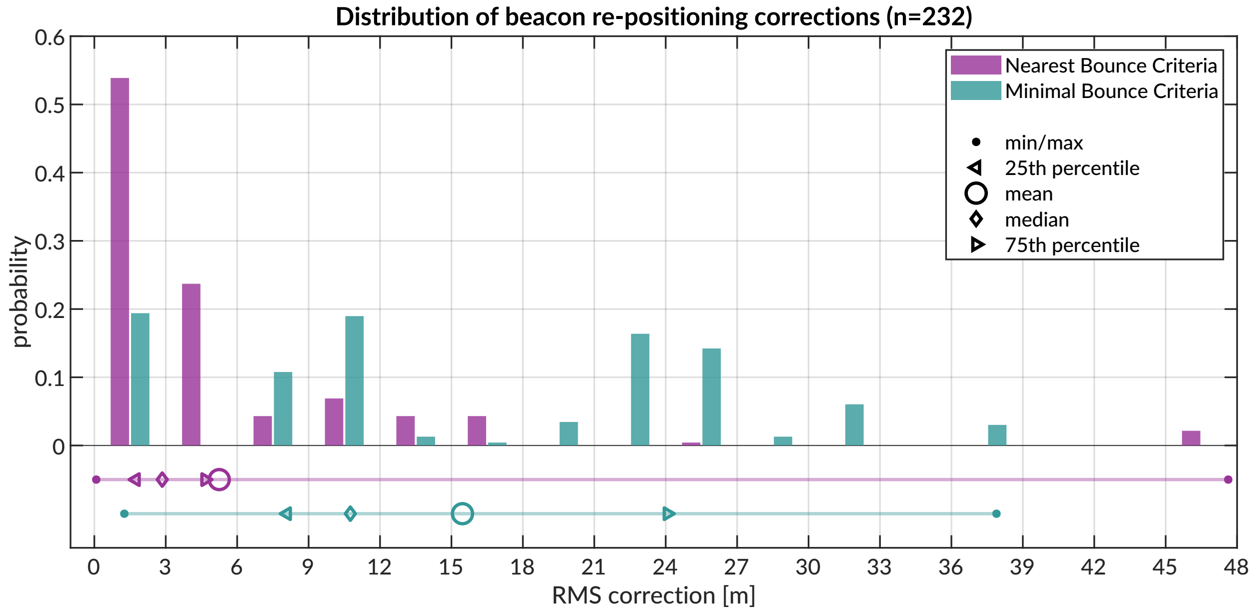

FIG. 11. Trilateration events; however, 264 entries are 2-beacon solutions, 22 are 3-beacon, and 2 are 4-beacon. When limited to only two ranging circles, the trilateration chooses the closer of the two intersection points. The x-axis is cut off at the upper limit for the NBC algorithm.

In several events, the MBC is unable to accurately estimate the effective sound speed for one of the acoustic links, leading to a large positioning error. The NBC, however, better resolves an approximation of the acoustic path. For example, in some trilateration solutions for the Eastern buoy, the MBC shows a correction of more than a kilometer; the NBC is two order of magnitudes less.

B. Re-navigating AUV *Macrura*

Up to this point, pseudorange estimation and localization have been evaluated on GPS-linked beacon-to-beacon connections to validate the NBC algorithm. This analysis ports the MBC and NBC algorithms to re-navigate the AUV *Macrura*.

The AUV dataset clearly exhibits instances where a receiver detects the same transmission more than once. This is not surprising considering the complex multipath provided by the Beaufort Lens. The 11 hour vehicle mission contains 3260 transmissions, 12938 total detections, and 4704 successful receptions. Allowing receptions with PSK errors would almost double the number of recorded multipath arrivals exploited for positioning, if a real-time solution could correctly parse paths from different arrivals in the same thirty-second cycle. Thus it remains a future endeavor to explore how failure mode information from acoustic modems could be used to identify unsuccessful but otherwise trustworthy arrivals to augment trilateration samples.

The following performance analysis is constrained to what the vehicle acted on in real-time. AUV *Macrura* and the ICNN ran an adaptive depth behavior to maintain acoustic communication on the insight that cross-layer links were more likely to fail than same-layer ones. Accordingly, the vehicle dove deeper than 50 meters about 20% of the time it was underway.

In contrast to the modem tests, where position correction illustrated re-positioning accuracy, the re-navigation corrections are less valuable in the absence of GNSS ground truth. The correction magnitude necessarily depends on the vehicle's internal navigation estimate, which is prone to larger errors from sensor drifts, ocean currents, and other error not captured in the hydrodynamic model. Thus, larger corrections are not necessarily indicative of worse performance. Navigation accuracy may be better described by trilateration error, the RMS of the remaining pseudorange errors from each acoustic link.

Fig. 12 shows the correction magnitudes and trilateration errors for events with three or more receptions during AUV operations. Whereas the MBC has a fairly bimodal nature, with peaks centered around 10–15 and 35–40 m, the NBC favors smaller corrections, from 5–20 m, and has a long tail. The distribution of corrections are much larger than the distribution of RMS error. It is apparent that, while both methods are quite successful, there is strong evidence that the NBC achieves single meter accuracy.

C. Investigating potential GNSS noise

The fact that the bulk of the best performing re-navigation error exists within the precision of the GNSS unit deployed invites a further look into GNSS noise. In the Arctic, GNSS performance worsens due to poor constellation coverage, larger ionospheric effects, and multipath interference. The National Security Implications of Climate Change for U.S. Naval Forces (Council, 2011) details some of the limitations of the Global Positioning System (GPS) at polar latitudes. Radio infrastructure that provides position corrections and references does not regularly extend to polar regions. The effect is minor for surface platform navigation —roughly 15 m of horizontal precision has been displayed at the North Pole—but is significant enough to register against the modem's detected travel times. Figure 13 zooms in on the GNSS and OWTT noise relative to the ice movement for two pairs of modem buoy connections. The two panels indicate the GPS drift as $\delta R = \sqrt{\delta x^2 + \delta y^2}$ and temporal drift, δt, relative to the median OWTT recorded between the two modems. The dashed line is scaled by a group velocity of 1440 m/s, such that if there were ideal sensor measurements with no drift, all events should exist on or near the line.

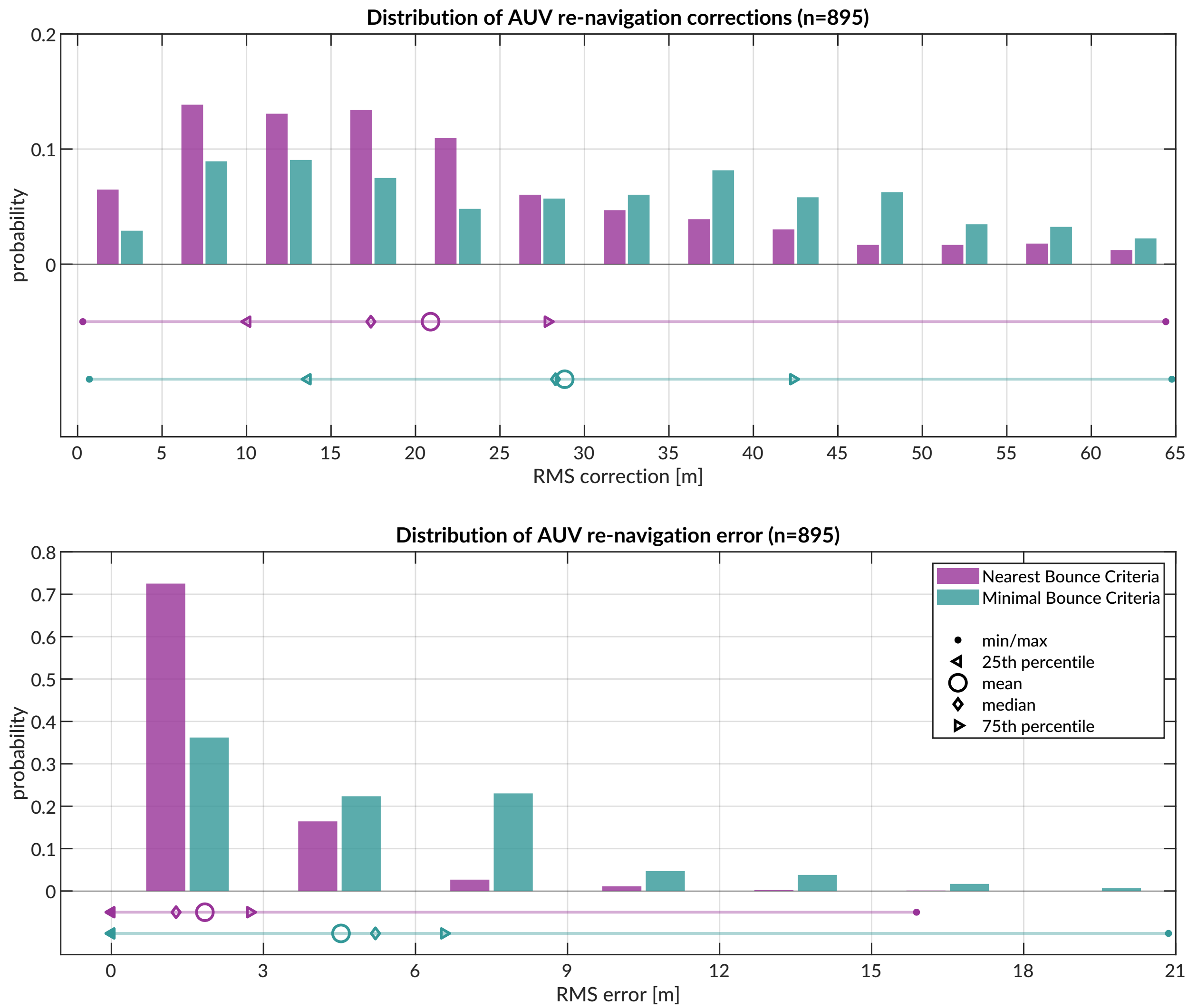

FIG. 12. Distribution of vehicle re-navigation corrections (top) and error (bottom) computed in post-processing for the Minimum and Nearest Bounce Criterion.

The top panel shows the connections between the North and East buoys. There is relative, i.e. non-rigid, ice movement between the North and East buoys, evidenced by events spanning the dashed line. But the height of the scatter plot is indicative of the precision of the GPS signal, as it remains consistent across many arrival time bands. Naturally, some minor offsets between these vertical bands relate to different operational configurations of

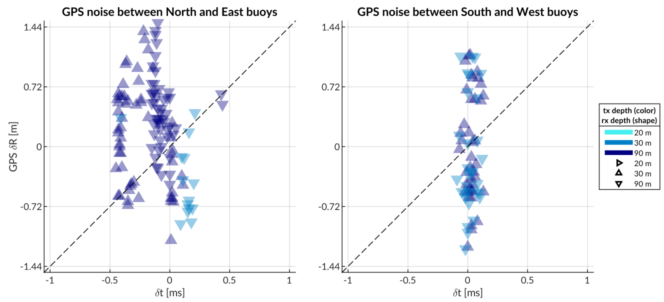

FIG. 13. A comparison of GPS drift (y-axis) versus OWTT drift (x-axis), colored by source and receiver depth. The physical link between North and East are shown on the top; South and West is on the bottom.

source and receiver depth. However, the large majority of events show vertical banding for the same nominal δt, indicating the amount of GPS drift.

This idea of GPS drift relative to the same OWTT measurements is further indicated by events between the other two buoys, South and West, in the bottom panel. These buoys are moving in a more rigid ice floe and there is minimal impact by source and receiver depth on the spread of OWTT. The GPS drift is much larger relative to the OWTT drift, which is sensitive to acoustic scattering, multipath, and/or environmental microstructure.

These are just two subsets of the physical links that cover all four GPS modem buoys. The GPS at camp is the least accurate due to the human activity and infrastructure occluding the physical puck.

VI. DISCUSSION

Given the computational constraints of real-time modeling, the gridded approach facilitates enough multipath classification to build in a "ray ensemble" of characteristic group velocities. This result is not always possible when aiming to find eigenrays to just an individual point, even with a higher density of launch angles. An important takeaway for those interested in ray-based localization is leveraging a local grid to give BELLHOP tolerance for finding solutions that otherwise may not be found in a center or single point solution. The limitations of numerical computation, particularly for a complex environment, are more adeptly addressed by accepting some uncertainty in position than by prescribing an exact solution. Even though BELLHOP is a greedy estimator for eigenrays, the additional data created is a negligible burden.

Underwater navigation research is broadly motivated by acquiring GPS-like navigation accuracy in GPS-denied conditions. The Arctic, while remote, is the perfect place to test mature navigation technologies in real GPS-denied conditions.

Range estimation is an essential step of acoustic localization and navigation. Current approaches in real-time underwater acoustic navigation simplify the non-linear relationship between a sound speed profile and acoustic propagation with a deterministic sound speed. Some post-processing approaches attempt to leverage the acoustic arrival structure via various ray methods, but often use a singular SSP for simplicity, even over long term missions or dynamic conditions. Thus, the conversion from travel time to range, particularly for real-time vehicle deployments, can be pre-conditioned for error growth as the OWTT/range increases.

For GPS-denied navigation, especially in hostile environments like the Arctic, tolerance for error is close to none. This work addresses a critical need in acoustic navigation by retooling acoustic arrival methods generally deemed too complex or labor intensive for real-time, ray-based range estimation to achieve GPS-like positioning.

We hypothesize and validate that the embedded stochastic prediction of a single group velocity is a smoothly varying function of range, source and receiver depth pairings, as well as multipath structure. We employ a GPS-tracked experiment to have a ground truth comparison for real-time localization algorithms. The real-time system achieves GPS-like navigation for an AUV without taking into account multipath structure; the ranging error improves by an order of magnitude with the suggested multipath adaptability, minimizing range error to single meters. Post-processing analysis shows that this method of ranging is sensitive to GPS drift itself; thus embedding a stochastic prediction of the horizontal group velocity has an outsized benefit to minimizing trilateration error.

There are many avenues through which this approach can be further refined and tested for field operations. Amongst them is defining the uncertainty grid for BELLHOP via stochastic or data-driven measures such as the distance traveled by the AUV between ICNN updates or the magnitude of the position corrections by the ICNN. Another is to entirely remove the seeded range and instead rely on the submerged asset's depth and recorded OWTT to find high probability fields in range.

The literature in underwater acoustic navigation and positioning is either real-time or physics-based. In this paper we demonstrate a field-tested approach that is both real-time and physics-based; this is achieved by coupling data streams with fast acoustic modeling. The methods exploit the upward refracting nature and the total ice cover of the Arctic environment to achieve remarkable ranging accuracy and precision. It transforms multipath, widely considered as an obstacle for acoustic ranging, into a new information content to refine ranging accuracy. We believe that this work enables more accurate range estimation, localization, and/or navigation for any field experiment given known source and receiver depths.

Performance in other acoustic environments may require introducing a different thresholded metric to sort time of arrivals. Given the NBC algorithm's improvement with increased multipath, its effectiveness is likely only challenged by the valid operational scales of a range independent propagation environment. For mesoscale operations, like that of many gliders, the group velocity criteria may need to be modified to better account for variability driven by range dependent propagation through internal waves, eddies, or even bathymetric changes like underwater volcanoes. BELLHOP simulations provide other relevant eigenray information, like time and angle of arrival, that is ripe for statistical and machine learning methods to classify a representative group velocity. A bespoke and fast ray tracing method, which was used during ICEX20 to evaluate the acoustic fit of sound speed profile parameterization (Bhatt *et al.*, 2022), can easily report back the number of turning points instead of the number of bounces for multipath classification.

This approach will start to break down in extremely dynamic environments, like fast moving fronts. Realistic *in situ* considerations of the acoustic environment may not be possible without complete through-the-sensor integration of acoustic dat and/or hyper realistic ocean models.

Many approaches to underwater navigation combine it with acoustic tomography, i.e., a joint estimation of both source and receiver locations and the ocean volume between them. There has been considerable success at this effort in post-processing methods, which utilize intensive—and due to the non-linearity of sound propagation, often brute force—computational methods. For vehicle operations, fast tomography is the ideal implementation, in that one can fully consider how sound speed structure, horizontally and vertically, influences sound propagation. AUVs can serve as moving sources to better image the ocean volume (Deffenbaugh, 1997; Elisseeff *et al.*, 2002), where mobile tomography and navigation converge on the same set of component technologies: position estimation, sound speed parameterization estimation, ray path identification, and vehicle path optimization.

But there are overwhelming challenges, operationally and computationally, for fast, mobile tomography to become a realistic endeavor. Addressing the spatial and temporal scales of what can be solved deterministically and what must be solved stochastically imposes a resolution constraint on the utility of gridded models—resolving fine features inaccurately (or with a false sense of confidence) could be more harmful than assuming range independence. Given that AUV operations are often on small spatial and temporal scales, the added benefit of a gridded model is quite small, and in cases like the Arctic, may actually mischaracterize the ocean volume. For gliders, with longer and larger operational scales, an ocean model may provide more useful information. Currently gliders are low power and do not have the storage or computational power to run a full-scale, realistic ocean model. A lightweight representation of the key environmental and acoustic features, passed through the same manner of acoustic message from the modem experiment, may drastically improve glider navigation.

ACKNOWLEDGMENTS

We acknowledge the significant operational effort spearheaded by the LAMSS ICEX20 team and all our collaborators. Bhatt was funded by a National Defense, Science, and Engineering Graduate Fellowship. This work was supported by the Office of Naval Research 322-OA under ICEX20 (N00014-17-1-2474) and Task Force Ocean (N00014-19-1-2716).

Ballard, M. S., Badiey, M., Sagers, J. D., Colosi, J. A., Turgut, A., Pecknold, S., Lin, Y.-T., Proshutinsky, A., Krishfield, R., Worcester, P. F., and Dzieciuch, M. A. (**2020**). "Temporal and spatial dependence of a yearlong record of sound propagation from the Canada Basin to the Chukchi Shelf," The Journal of the Acoustical Society of America **148**(3), 1663–1680, http://asa.scitation.org/doi/10.1121/10.0001970http://files/814/Ballardetal.-2020-Temporalandspatialdependenceofayearlongreco.pdf, doi: 10.1121/10.0001970.

Barker, L. D. L., Jakuba, M. V., Bowen, A. D., German, C. R., Maksym, T., Mayer, L., Boetius, A., Dutrieux, P., and Whitcomb, L. L. (**2020**). "Scientific challenges and present capabilities in underwater robotic vehicle design and navigation for oceanographic exploration under-ice," Remote Sensing **12**(16), 1–31, doi: 10.3390/RS12162588.

Bellingham, J., Leonard, J., Vaganay, J., Goudey, C., Atwood, D., Consi, T., Bales, J., Schmidt, H., and Chryssostomidis, C. (**1995**). "Auv operations in the arctic," in *Sea Ice Mechanics and Arctic Modeling Workshop*.

Bhatt, E. C. (**2021**). "A Virtual Ocean framework for environmentally adaptive, embedded acoustic navigation on autonomous underwater vehicles," Ph.D. thesis, Massachusetts Institute of Technology and Woods Hole Oceanographic Institution Joint Program, https://hdl.handle.net/1912/27309, doi: 10.1575/1912/27309.

Bhatt, E. C., Howard, B., and Schmidt, H. (**2022**). "An Embedded Tactical Decision Aid Framework for Environmentally Adaptive Autonomous Underwater Vehicle Communication and Navigation," IEEE Journal of Oceanic Engineering .

Brooke, J. (**1981**). "Arcs (autonomous remotely controlled submersible)," in *Proceedings of the 1981 2nd International Symposium on Unmanned Untethered Submersible Technology*, IEEE, Vol. 2, pp. 28–28.

Chassignet, E. P., Hurlburt, H. E., Smedstad, O. M., Halliwell, G. R., Hogan, P. J., Wallcraft, A. J., Baraille, R., and Bleck, R. (**2007**). "The HYCOM (HYbrid Coordinate Ocean Model) data assimilative system," Journal of Marine Systems **65**(1-4), 60–83, doi: 10.1016/J.JMARSYS.2005.09.016.

Chen, R., Poulsen, A., and Schmidt, H. (**2019**). "Spectral, spatial, and temporal characteristics of underwater ambient noise in the Beaufort Sea in 1994 and 2016," The Journal of the Acoustical Society of America **145**(2), 605–614, https://asa.scitation.org/doi/full/10.1121/1.5088601http://files/757/Chenetal.-2019-Spectral,spatial,andtemporalcharacteristicsof.pdf, doi: 10.1121/1.5088601.

Chen, R., and Schmidt, H. (**2020**). "Temporal and spatial characteristics of the Beaufort Sea ambient noise environment," The Journal of the Acoustical Society of America **148**(6), 3928–3941, https://asa.scitation.org/doi/full/10.1121/10.0002955http://files/755/ChenandSchmidt-2020-TemporalandspatialcharacteristicsoftheBeaufo.pdf, doi: 10.1121/10.0002955.

Claus, B., Kepper, J. H., Suman, S., and Kinsey, J. C. (**2018**). "Closed-loop one-way-travel-time navigation using low-grade odometry for autonomous underwater vehicles," Journal of Field Robotics **35**(4), 421–434, doi: 10.1002/rob.21746.

Council, N. R. (**2011**). *National Security Implications of Climate Change for U.S. Naval Forces* (The National Academies Press, Washington, DC), https://www.nap.edu/catalog/12914/national-security-implications-of-climate-change-for-us-naval-forces.

Deffenbaugh, M. (**1997**). "Optimal Ocean Acoustic Tomography and Navigation with Moving Sources," Ph.D. thesis, MIT-WHOI Joint Program in Oceanography/Applied Ocean Science and Engineering.

Deffenbaugh, M., Bellingham, J. G., and Schmidt, H. (**1996**a). "Relationship between spherical and hyperbolic positioning," Oceans Conference Record (IEEE) **2**, 590–595, doi: 10.1109/OCEANS.1996.568293.

Deffenbaugh, M., Schmidt, H., and Bellingham, J. G. (**1996**b). "Acoustic positioning in a fading multipath environment," in *OCEANS 96 MTS/IEEE Conference Proceedings. The Coastal Ocean-Prospects for the 21st Century*, IEEE, Vol. 2, pp. 596–600.

Duda, T. F., Morozov, A. K., Howe, B. M., Brown, M. G., Speer, K., Lazarevich, P., Worcester, P. F., and Cornuelle, B. D. (**2006**). "Evaluation of a long-range joint acoustic navigation / thermometry system," in *Oceans 2006*, pp. 1–6, http://files/939/Dudaetal.-2006-EvaluationofaLong-RangeJointAcousticNavigati.pdfhttp://files/940/4099137.html, doi: 10.1109/OCEANS.2006.306999.

Duda, T. F., Zhang, W. G., and Lin, Y.-T. (**2021**). "Effects of Pacific Summer Water layer variations and ice cover on Beaufort Sea underwater sound ducting," The Journal of the Acoustical Society of America **149**(4), 2117–2136, doi: 10.1121/10.0003929.

Duda, T. F., Zhang, W. G., Lin, Y.-T., and Newhall, A. E. (**2019**). "Long-range sound propagation in the Canada Basin," http://files/565/Dudaetal.-Unknown-LONG-RANGESOUNDPROPAGATIONINTHECANADABASIN.pdf.

Elisseeff, P., Schmidt, H., and Xu, W. (**2002**). "Ocean acoustic tomography as a data assimilation problem," IEEE Journal of Oceanic Engineering **27**(2), 275–282, http://files/438/Elisseeff,Schmidt,Xu-2002-OceanAcousticTomographyasaDataAssimilationProblem.pdf, doi: 10.1109/JOE.2002.1002482.

Eustice, R. M., Whitcomb, L. L., Singh, H., and Grand, M. (**2006**). "Recent advances in synchronous-clock one-way-travel-time acoustic navigation," Oceans 2006 doi: 10.1109/OCEANS.2006.306931.

Eustice, R. M., Whitcomb, L. L., Singh, H., and Grund, M. (**2007**). "Experimental results in synchronous-clock one-way-travel-time acoustic navigation for autonomous underwater vehicles," in *Proceedings - IEEE International Conference on Robotics and Automation*, pp. 4257–4264, http://files/877/Eusticeetal.-2007-ExperimentalResultsinSynchronous-ClockOne-Way-.pdfhttp:

//files/878/4209752.html, doi: 10.1109/ROBOT.2007.364134.

Fossum, T. O., Norgren, P., Fer, I., Nilsen, F., Koenig, Z. C., and Ludvigsen, M. (**2021**). "Adaptive sampling of surface fronts in the arctic using an autonomous underwater vehicle," IEEE Journal of Oceanic Engineering **46**(4), 1155–1164, doi: 10.1109/JOE.2021.3070912.

Freitag, L., Ball, K., Partan, J., Koski, P., and Singh, S. (**2016**). "Long range acoustic communications and navigation in the Arctic," OCEANS 2015 - MTS/IEEE Washington 2–6, doi: 10.23919/oceans.2015.7401956.

Graupe, C. E., Van Uffelen, L. J., Webster, S. E., Worcester, P. F., and Dzieciuch, M. A. (**2019**). "Preliminary results for glider localization in the Beaufort Duct using broadband acoustic sources at long range," in *OCEANS 2019 MTS/IEEE Seattle, OCEANS 2019*, pp. 1–6, http://files/763/Graupeetal.-2019-Preliminaryresultsforgliderlocalizationinthe.pdfhttp://files/912/Graupeetal.-2019-Preliminaryresultsforgliderlocalizationinthe.pdfhttp://files/764/8962637.htmlhttp://files/913/8962637.html, doi: 10.23919/OCEANS40490.2019.8962637.

Hayes, D. R., and Morison, J. H. (**2002**). "Determining turbulent vertical velocity, and fluxes of heat and salt with an autonomous underwater vehicle," Journal of Atmospheric and Oceanic Technology **19**(5), 759–779.

Howe, B. M., Miksis-Olds, J., Rehm, E., Sagen, H., Worcester, P. F., and Haralabus, G. (**2019**). "Observing the Oceans Acoustically," Frontiers in Marine Science **6**, 426, https://www.frontiersin.org/article/10.3389/fmars.2019.00426/full, doi:

10.3389/fmars.2019.00426.

Jackson, E. (**1983**). "Autonomous remotely controlled submersible "ARCS"," in *Proceedings of the 1983 3rd International Symposium on Unmanned Untethered Submersible Technology*, IEEE, Vol. 3, pp. 77–88.

Jakuba, M. V., Roman, C. N., Singh, H., Murphy, C., Kunz, C., Willis, C., Sato, T., and Sohn, R. A. (**2008**). "Long-baseline acoustic navigation for under-ice autonomous underwater vehicle operations," Journal of Field Robotics **25**(11-12), 861–879, https://onlinelibrary.wiley.com/doi/full/10.1002/rob.20250https://onlinelibrary.wiley.com/doi/abs/10.1002/rob.20250https://onlinelibrary.wiley.com/doi/10.1002/rob.20250, doi: 10.1002/ROB.20250.

Kepper, J. H., Claus, B. C., and Kinsey, J. C. (**2017**). "MEMS IMU and one-way-travel-time navigation for autonomous underwater vehicles," in *OCEANS 2017 - Aberdeen*, Vol. 2017-Octob, pp. 1–9, http://files/550/Kepper,Claus,Kinsey-2017-MEMSIMUandOne-Way-Travel-TimeNavigationforAutonomousUnderwaterVehicles.pdf, doi: 10.1109/OCEANSE.2017.8084842.

Krishfield, R., Toole, J., Proshutinsky, A., and Timmermans, M. L. (**2008**). "Automated ice-tethered profilers for seawater observations under pack ice in all seasons," Journal of Atmospheric and Oceanic Technology **25**(11), 2091–2105, doi: 10.1175/2008JTECHO587.1.

Kukulya, A., Plueddemann, A., Austin, T., Stokey, R., Purcell, M., Allen, B., Littlefield, R., Freitag, L., Koski, P., Gallimore, E. *et al.* (**2010**). "Under-ice operations with a remus-100 auv in the arctic," in *2010 IEEE/OES Autonomous Underwater Vehicles*, IEEE, pp. 1–8.

Kunz, C., Murphy, C., Camilli, R., Singh, H., Bailey, J., Eustice, R., Jakuba, M., Nakamura, K., Roman, C., Sato, T., Sohn, R., and Willis, C. (**2008**). "Deep sea underwater robotic exploration in the ice-covered Arctic ocean with AUVs," in *2008 IEEE/RSJ International Conference on Intelligent Robots and Systems*, IEEE, pp. 3654–3660, http://files/875/Kunzetal.-2008-Deepseaunderwaterroboticexplorationintheice.pdfhttp://files/968/Kunzetal.-2008-Deepseaunderwaterroboticexplorationintheice.pdfhttp://ieeexplore.ieee.org/document/4651097/, doi: 10.1109/IROS.2008.4651097.

Light, R., and Morison, J. (**1989**). "The autonomous conductivity-temperture vehicle: First in the seashuttle family of autonomous underwater vehicle's for scientific payloads," in *Proceedings OCEANS*, Vol. 3, pp. 793–798, doi: 10.1109/OCEANS.1989.586683.

Litvak, A. (**2015**). "Acoustics of the deepwater part of the arctic ocean and of russia's arctic shelf," Herald of the Russian Academy of Sciences **85**, 239–250, doi: 10.1134/S1019331615030144.

Mikhalevsky, P. N., Sperry, B. J., Woolfe, K. F., Dzieciuch, M. A., and Worcester, P. F. (**2020**). "Deep ocean long range underwater navigation," The Journal of the Acoustical Society of America **147**(4), 2365–2382, http://asa.scitation.org/doi/10.1121/10.0001081http://files/631/Mikhalevskyetal.-2020-Deepoceanlongrangeunderwaternavigation.pdf, doi: 10.1121/10.0001081.

Norgren, P., Lubbad, R., and Skjetne, R. (**2014**). "Unmanned underwater vehicles in Arctic operations," in *22nd IAHR International Symposium on Ice*.

Paull, L., Saeedi, S., Seto, M., and Li, H. (**2014**). *AUV navigation and localization: A review*, **39**, pp. 131–149, http://files/127/Paulletal.-2014-AUVnavigationandlocalizationAreview.pdf.

Plueddemann, A. J., Kukulya, A. L., Stokey, R., and Freitag, L. (**2012**). "Autonomous Underwater Vehicle Operations Beneath Coastal Sea Ice," IEEE/ASME Transactions on Mechatronics **17**(1), 54–64, doi: 10.1109/TMECH.2011.2174798 conference Name: IEEE/ASME Transactions on Mechatronics.

Porter, M. B. (**2011**). "The BELLHOP Manual and User's Guide," HLS Research, , 2010 1–57, http://oalib.hlsresearch.com/Rays/HLS-2010-1.pdf.

Poulsen, A. J., and Schmidt, H. (**2017**). "Acoustic noise properties in the rapidly changing Arctic Ocean," **070005**(2016), 070005, doi: 10.1121/2.0000552.

Randeni, S., Schneider, T., and Schmidt, H. (**2020**). "Construction of a high-resolution under-ice AUV navigation framework using a multidisciplinary virtual environment," in *2020 IEEE/OES Autonomous Underwater Vehicles Symposium, AUV 2020*, pp. 1–7, http://files/689/Randenietal.-2020-Constructionofahigh-resolutionunder-iceAUVna.pdf, doi: 10.1109/AUV50043.2020.9267950.

Randeni, S., Schneider, T., Schmidt, H., Bhatt, E., and Viquez, O. (**2021**). "A high-resolution AUV navigation framework with integrated communication and tracking for under-ice deployments," Field Robotics (in review).

Rossby, T., Dorson, D., and Fontaine, J. (**1986**). "The RAFOS System," Journal of Atmospheric and Oceanic Technology **3**, 148–162.

Rypkema, N. R., Fischell, E. M., and Schmidt, H. (**2017**). "One-Way Travel-Time Inverted Ultra-Short Baseline Localization for Low-Cost Autonomous Underwater Vehicles," in *2017 IEEE International Conference on Robotics and Automation (ICRA)*, Singapore, pp. 4920–4926.

Schmidt, H., and Schneider, T. (**2016**). "Acoustic communication and navigation in the new Arctic-A model case for environmental adaptation," 3rd Underwater Communications and Networking Conference, Ucomms 2016 http://files/583/Schmidt,Schneider-2016-AcousticCommunicationandNavigationintheNewArctic-AModelCaseforEnvironmen pdfhttp://files/614/2012JOE001161R.pdf, doi: 10.1109/UComms.2016.7583469.

Schneider, T., and Schmidt, H. (**2018**). "NETSIM: A realtime virtual ocean hardware-in-the-loop acoustic modem network simulator," in *2018 4th Underwater Communications and Networking Conference, UComms 2018*, pp. 1–5, http://files/1047/SchneiderandSchmidt-2018-NETSIMARealtimeVirtualOceanHardware-in-the-l.pdfhttp://files/1048/8493188.html, doi: 10.1109/UComms.2018.8493188.

Schneider, T., Schmidt, H., and Randeni, S. (**2020**). "Self-Adapting Under-Ice Integrated Communications and Navigation Network," 2020 5th Underwater Communications and Networking Conference, UComms 2020 5, http://files/607/Schneideretal.-Self-AdaptingUnder-IceIntegratedCommunications.pdf.

Singh, S., Grand, M., Bingham, B., Eustice, R., Singh, H., and Freitag, L. (**2006**). "Underwater acoustic navigation with the WHOI Micro-Modem," in *Oceans 2006*, IEEE, pp. 1–4, http://ieeexplore.ieee.org/document/4099008/http://files/774/Singhetal.-2006-UnderwaterAcousticNavigationwiththeWHOIMicro.pdf, doi: 10.

1109/OCEANS.2006.306853.

Timmermans, M.-L., and Winsor, P. (**2013**). "Scales of horizontal density structure in the chukchi sea surface layer," Continental Shelf Research **52**, 39–45.

Toole, J. M., Krishfield, R. A., Timmermans, M. L., and Proshutinsky, A. (**2011**). "The Ice-Tethered profiler: Argo of the Arctic," Oceanography **24**(3), 126–135, doi: 10.5670/oceanog.2011.64.

Uffelen, L. J. V., Howe, B. M., Nosal, E.-M., Carter, G. S., Worcester, P. F., and Dzieciuch, M. A. (**2016**). "Localization and subsurface position error estimation of gliders using broadband acoustic signals at long range," IEEE Journal of Oceanic Engineering **41**(3), 501–508.

Van Uffelen, L. J. (**2021**). "Global Positioning Systems: Over Land and Under Sea," Acoustics Today **17**(1), 52, doi: 10.1121/at.2021.17.1.52.

Van Uffelen, L. J., Nosal, E.-M., Howe, B. M., Carter, G. S., Worcester, P. F., Dzieciuch, M. A., Heaney, K. D., Campbell, R. L., and Cross, P. S. (**2013**). "Estimating uncertainty in subsurface glider position using transmissions from fixed acoustic tomography sources," The Journal of the Acoustical Society of America **134**(4), 3260–3271, doi: 10.1121/1.4818841.

Webster, S. E., Eustice, R. M., Singh, H., and Whitcomb, L. L. (**2009**). "Preliminary deep water results in single-beacon one-way-travel-time acoustic navigation for underwater vehicles," 2009 IEEE/RSJ International Conference on Intelligent Robots and Systems, IROS 2009 2053–2060, http://files/416/Websteretal.-2009-Preliminarydeepwaterresultsinsingle-beaconone-way-travel-timeacousticnavigationf pdf, doi: 10.1109/IROS.2009.5354457.

Webster, S. E., Eustice, R. M., Singh, H., and Whitcomb, L. L. (**2012**). "Advances in single-beacon one-way-travel-time acoustic navigation for underwater vehicles," International Journal of Robotics Research **31**(8), 935–950, doi: 10.1177/0278364912446166.

Webster, S. E., Freitag, L. E., Lee, C. M., and Gobat, J. I. (**2015**). "Towards real-time under-ice acoustic navigation at mesoscale ranges," in *Proceedings - IEEE International Conference on Robotics and Automation*, June, IEEE, pp. 537–544, http://files/625/Websteretal.-2015-Towardsreal-timeunder-iceacousticnavigationat.pdfhttp://files/641/Websteretal.-2015-Towardsreal-timeunder-iceacousticnavigationat.pdfhttp://files/835/Websteretal.-2015-Towardsreal-timeunde, doi: 10.1109/ICRA.2015.7139231.

Wu, M., Barmin, M. P., Andrew, R. K., Weichman, P. B., White, A. W., Lavely, E. M., Dzieciuch, M. A., Mercer, J. A., Worcester, P. F., and Ritzwoller, M. H. (**2019**). "Deep water acoustic range estimation based on an ocean general circulation model: Application to PhilSea10 data," The Journal of the Acoustical Society of America **146**(6), 4754–4773, https://asa.scitation.org/doi/10.1121/1.5138606http://files/947/Wuetal.-2019-Deepwateracousticrangeestimationbasedonano.pdfhttp://files/948/1.html, doi: 10.1121/1.5138606.